Will low primary production rates in the Amundsen Basin (Arctic Ocean) remain low in a future ice-free setting, and what governs this production?

Lars Chresten Lund-Hansen[a,b,*], Jørgen Bendtsen[c], Tanja Stratmann[b,f], Rasmus Tonboe[d], Steffen Malskær Olsen[d], Stiig Markager[e], Brian K. Sorrell[b],

[a]Arctic Research Center, Bioscience, Aarhus University, Ny Munkegade 114, Build. 1540, 8000 Aarhus C, Denmark

[b]Aquatic Biology, Bioscience, Aarhus University, Ole Worms Allé 1, Build. 1134, 8000 Aarhus C, Denmark

[c]Climatelab, Symbion Science Park, Fruebjergvej 3, Box 98, 2100 Copenhagen O, Denmark

[d]Danish Meteorological Institute, Lyngbyvej 100, 2100 Copenhagen O, Denmark

[e]Marine Ecology, Bioscience, Aarhus University, Frederiksborgvej 399, 4000 Roskilde, Denmark

[f]NIOZ Royal Netherlands Institute for Sea Research, Department of Estuarine and Delta Systems, Utrecht University, P.O. Box 140, 4400 AC Yerseke, The Netherlands

* Corresponding author

E-mail address: lund-hansen@bios.au.dk (L.C. Lund-Hansen).

ABSTRACT

The study is based on a very extensive data-set of physical, biological, and optical parameters from below the sea ice in the western Amundsen Basin, central Arctic Ocean, in August-September 2012 during the record low sea ice extent. The water column was strongly stratified at all stations related to salinity differences between a surface layer of reduced salinities (< 29-33) and deep-water layer salinities (> 34). A nitrate utilization-based budget in the surface layer gave a primary production of 67.5 mg C m^{-2} d^{-1}, which reduced to 3.9 mg C m^{-2} d^{-1} in August 2012. Amundsen Basin primary production rates are lower than rates determined for other Arctic Ocean deep-water basins, and also lower compared to rates on the shelf. Below ice phytoplankton was well adapted to low light conditions in the Amundsen Basin and the photosynthetic potential was high, but limited by the low nutrient fluxes induced by the strong stratification. Amundsen Basin is foreseen to be ice-free in summer in 3-4 decades, and the question whether primary production will increase when ice-free was resolved with a coupled physical-biogeochemical model. Results showed that production will increase 10 to 14 times from the present 3.9 mg C m^{-2} d^{-1} to 37.4 and 55.2 mg C m^{-2} d^{-1} for an ice-free August and July-August, respectively. The study substantiates that both present and future ice-free low production rates were related to the strong stratification, reduced nutrient fluxes, and deep lying nutrient rich waters. Low production rates and strong stratification are discussed in the view of parameters that increase this stratification as higher freshwater run off or reduce stratification as wind.

Keywords: Arctic Ocean, Primary production, Stratification, Nutrients, PAR, Ice-free

1. Introduction

The Arctic Ocean has experienced a gradual decrease in summer sea ice extent since at least 1977 (Overland et al., 2013; Serreze et al., 2007) and a record minimum of $2.3 \cdot 10^6$ km^2 was reached in September 2012 (Serezze et al., 2016). Sea ice thickness has also decreased from about 2-3 m to about 1.5 m during the same period (Laxon et al., 2013). It is foreseen that the Arctic Ocean will be ice-free within 3-4 decades, modified by some regional differences such as areas with multi-year ice north of Greenland (Laliberté et al., 2016). Large shelf areas of the Arctic Ocean, such as the Barents, Kara, Laptev, Siberian, Chukchi, and Beaufort Seas, are already ice-free in summer (Arrigo and Dijken, 2015) as well as large parts of the Canada Basin (Ardyna et al. 2014). Primary production rates in the sea ice-covered central Arctic Ocean reach 117 mg C m^{-2} d^{-1} (Rao and Platt, 1984), 106 mg C m^{-2} d^{-1} in the Canada Basin (Lee and Whitledge, 2005), and 56 mg C m^{-2} d^{-1} in the Nansen Basin based on a productive period of 90 days (Sakshaug, 2004). In comparison, the Arctic shelf primary production rates are higher as seen in the Barents Sea (100-2000 mg C m^{-2} d^{-1}, Rey et al., 1987), the Bering Strait and Chukchi Sea (100-3600 mg C m^{-2} d^{-1} Lee et al., 2007; Barber et al., 2015), though lower on the Canadian shelf (200-600 mg C m^{-2} d^{-1}) (Carmack et al., 2004). However, the total Arctic shelf primary production increased between 1998 and 2012 from 460 to 550 Tg C y^{-1} due to longer open water periods and increased upwelling of nutrients (Arrigo and Dijken, 2015). Whether the sea ice cover and a thereby reduced light and wind mixing are the only explanations for the significant lower primary production rates in central Arctic Ocean basins compared to the shelf areas, and whether basin production rates increase in a foreseen future ice-free summer, remain uncertain (Overland et al., 2013).

Primary production in the Arctic Ocean is thought to be governed by an interaction between stratification of the water column, light, and nutrients (Tremblay and Gagnon, 2009; Steinacher et al., 2010; Popova et al., 2012). A characteristic feature of the central Arctic Ocean is a low saline surface mixed layer (SML) with a marked halocline which inhibits vertical mixing (Popova et al., 2012), and is established by inflow of riverine freshwater (McCleland et al., 2012; Carmack et al., 2015) and sea ice melt (Rudels et al., 1996). Nutrients, particularly nitrogen compounds and silicate (Stratmann et al., 2017), are abundant at depths below the SML, but comparatively low in the SML layer in July-August (Codispoti et al., 2013; Slagstad et al., 2015) when the Arctic Ocean is likely to be ice-free in the future. During these ice-free summer months, the water column will be exposed to winds and an increased frequency of wind-induced mixing (Lincoln et al., 2016), which can bring new nutrients to the surface waters (Randelhoff et al., 2016) and promote higher primary production rates (Carmack et al., 2004; Tremblay and Gagnon, 2009; Tremblay et al., 2012). Irradiance below the ice is at present 5 to 10 percent of the surface irradiance (Lund-Hansen et al., 2015), which will increase to almost 100 percent at the surface of an ice-free water column. Exposure to winds and wind-induced mixing combined with a significantly higher irradiance will likely promote higher rates of primary production provided that nutrients are available (Carmack et al., 2004; Tremblay and Gagnon, 2009), as production is generally limited by nutrients in late summer (July-August) in the Arctic Ocean (Popova et al., 2012; Leu et al., 2011). The present study is based on a large number of stations within a limited and focused area in comparison to previous studies, that are either based on a few *in situ* data and measurements (Wheeler et al., 1996; Gosselin et al., 1997; Olli et al., 2007; Fernández-Méndez et al., 2015), pan-Arctic modelling of primary production (Jin et al., 2015; Slagstad et al.,2011; 2015; Zhang et al., 2010), or remote sensing (Hill et al., 2013). It comprises a compilation of CTD-data, nutrients, optics, and fluorescence-based photosynthetic parameters collected at stations in the western Amundsen Basin (> 87 °N) in the Eurasian part of the Arctic Ocean in late summer/early Autumn 2012, during the latest recorded minimum in sea cover (Serezze et al., 2016). Based on this we address two main questions: 1) What parameters govern the primary production in the Amundsen Basin and specifically in late summer, and 2)

Will rates of primary production increase in this basin in future ice-free summer months?

2. Materials and Methods

2.1. Study site and sampling

The Amundsen Basin is the largest (~ $4.4 \cdot 10^5$ km^2) and deepest (~ 4.000 m) basin of the Eurasian basins, located between the Gakkel and the Lomonosov Ridges, close to the North Pole (Fig. 1). Sampling was carried out in a section north of >87 °N and southeast of the Lomonosov Ridge in the western part of the Amundsen Basin during the Danish-Swedish joint LOMROG III cruise aboard the Swedish icebreaker *Oden* between 31 July and 14 September 2012. We obtained 26 CTD profiles, termed CTD stations, which were acquired from leads in the ice with a SBE19*plus*V2. Salinities are reported as practical salinity units. Water was sampled at 10, 20, 40, 60, 100, 150 and 200 m with a single 5 liter Niskin bottle for analyses of chlorophyll a (Chl *a*) and inorganic nutrients (NO_3^-, NO_2^-, NH_4^+, PO_4^{3-}, $Si(OH_4)$). At 27 further stations, here termed sea ice stations, water was sampled with a mechanical bilge pump with the water intake at 1-2 m below the sea ice bottom through a drilled 90 mm hole in the ice. Samples were likewise analyzed for nutrientsand Chl *a* as at the CTD stations. At sea ice stations, water was also collected for chlorophyll fluorescence yield analyses. All water samples were collected in cleaned polyethylene 2-4 liter containers and returned to the ship by helicopter in cold darkened cooling boxes. PAR transmittance through the ice and the diffuse PAR attenuation coefficient K_d(PAR) in the water column below the ice were derived at sea ice stations using cosine-corrected LiCor PAR sensors (Li-192) for air and water at all sea ice stations, following the procedures described by Lund-Hansen et al. (2015). A LiCor PAR sensor (Li-190) was mounted with a data-logger on top of the bridge of *Oden* to measure and log down-welling PAR every 5 minutes.

2.2. Laboratory analyses

Water samples for nutrients were filtered (0.4 µm Whatmann filters) in the ship laboratory and kept frozen (-21°C) until analysis at Aarhus University in Denmark after the cruise. Analyses followed standard procedures (Hansen and Koroleff, 1999) with detection limits: NO_3^-= 0.1 µmol L^{-1}, NO_2^- = 0.04 µmol L^{-1}, NH_4^+ = 0.3 µmol L^{-1}, PO_4^{3-} = 0.06 µmol L^{-1}, $Si(OH)_4$ = 0.2 µmol L^{-1}. Water samples for Chl *a* were filtered (0.3 µm Advantec GF75 filters) and filters were preserved in ethanol and kept frozen (-21°C) until analysis in Denmark immediately after the cruise. Fluorescence signals of Chl *a* dissolved in ethanol were measured on a calibrated Turner Design fluorometer (TD-700) and converted into concentrations based on a standard reference following Lund-Hansen et al. (2015). Absorbance at wavelengths 480 and 665 nm was also measured on samples using a spectrophotometer (Thermospectronic HELIOS λ), where the absorbance ratio 480:665 was applied as a proxy for nutrient limitation (Heath et al., 1990). A ratio < 2 indicates that algae photosynthesis is not limited by nutrients and conversely for a ratio >2 (Heath et al., 1990). The fluorescence signal measured with Seapoint fluorometer mounted on the CTD was converted into Chl *a* concentrations by means of a calibration of measured fluorescence signal at a specific depth compared to Chl *a* concentration at same depth. The calibration demonstrated a significant ($p < 0.001$) and strong correlation between measured fluorescence and Chl *a* concentrations ($r^2 = 0.72$, $n = 190$).

2.3. PAM-fluorometry

Variable chlorophyll fluorescence yield of the phytoplankton was examined on water samples using a Walz Phyto-PAM fluorometer, from which photosynthetic parameters were derived (Schrieber, 2010). Water samples from just below the sea ice (1-2 m) were incubated in the dark

for at least 0.5 hours before they were analyzed to ensure that all photosynthetic reaction centers were open (Schreiber et al., 1995). Samples were placed in the cuvette of the Phyto-PAM instrument, taking care that the laboratory was darkened, and the light was dimmed. Dark adapted minimum fluorescence yield (F_o) was determined first, followed by a measure of maximum fluorescence yield (F_m) during the application of a short (0.6 s) saturating irradiance pulse. Variable fluorescence (F_v) was calculated as $F_v = F_m - F_o$, and the maximum quantum yield (F_v/F_m) was calculated as $F_v/F_m = (F_m - F_o)/F_m$. In brief, F_v/F_m is a measure of photosynthetic health (Hawes et al., 2012). Relative electron transport (rETR) rates were determined based on the rapid light curve technique (RLC) with the Phyto-PAM (Ralph and Gademann, 2005), from where photosynthetic parameters α, $rETR_{maximum}$, and E_k were derived based on the Jassby and Platt (1976) equations.

2.4. Model description and sensitivity study

Nutrient fluxes and primary production were calculated from a one-dimensional water column model (COHERENS) where the 1D momentum and transport equations for temperature and salinity were solved (Luyten et al., 2014) with a new module for biogeochemical tracers included. The model was driven by meteorological fields of wind, air temperature, humidity and cloudiness based on NCEP-reanalysis data (Kalnay et al., 1996) for an Arctic location representative for the observations (88.90° N, 90.89° W). The biogeochemical module described the vertical distributions of nitrate (DIN), phytoplankton (P), and dissolved and particulate organic nitrogen (DON, PON). The model simulated the upper 200 m of the water column in the period from 1 July to 30 August 2012. Photosynthesis in the model was determined by Chl *a* concentrations (determined from P - the carbon content (Appendix A)), PAR, K_d(PAR), P^B_{max}, and α^B obtained from an ice-free area in August 2012 (Fernández-Mendéz et al., 2015). There was no wind or atmospheric heat exchange included during ice-covered periods, and the influence from melting and freezing of sea ice on salinity and temperature was excluded. The location was completely ice-covered in 2012 and a sensitivity study was performed with two scenarios characterized by ice-free conditions in (1) August and (2) July-August, respectively. These scenarios show the model response to ice-free conditions during a one or two-month period where the influence from increased insolation, wind forcing and heat exchange on stratification and primary production in the surface layer is considered. In addition, a scenario where PAR was increasedwas evaluated for estimating the relative importance of light- and nutrient-limitation. The model is described in detail in Appendix A.

3. Results

3.1. Surface mixed layer, chlorophyll a, nutrients, and stratification

CTD and sea ice stations covered the western and central part of the Amundsen Basin and about 40 percent of the total basin; both types of stations were placed randomly (Fig. 1). A compilation of the 26 CTD profiles (Fig. 2) shows the presence of a strongly stratified water column with a surface mixed layer (SML) down to about 21 m depth. From here, salinity gradually increased through the cold halocline layer (CHL) and reached a salinity of about 34.7 at 200 m depth (Fig. 2a) close to the top of Atlantic water with a salinity of 34.8 (Rudels et al., 1996). SML salinities varied between 29.5 and 33.1 and reflected the general decrease in SML salinity towards the Amerasian Basin (Serreze and Barry, 2014) with a salinity of 29.5 at station A (88° 03.58 N, 145° 16.56 E, Fig. 1) and 33.1 at station B (87° 28.24 N, 18° 58.52 , Fig. 1). There was a small variation in SML temperatures with a maximum difference of 0.19 °C between stations A (-1.57 °C) and B (-1.76 °C) with warmer SML water towards the Amerasian Basin. The trend of water density with depth is comparable to the salinity distribution, given very small temperature variations (Fig. 2c). Hence, the water column was stratified at all CTD stations, expressed by potential density

maximum and minimum differences of 2.81 and 0.94 kg m^{-3} between 10 and 60 m depth, respectively, with an increase in stratification towards the Amerasian Basin (Fig. 2a). There was a Chl *a* maximum of 0.2 mg m^{-3} in the surface of the SML, from where it gradually decreased to a background value of 0.02 mg m^{-3} at 200 m (Fig. 2d). The nutrients NO_2^-, NH_4^+, NO^-, PO_4^{3-} were all low in the SML < 20 m depth (NO_2^- = 0.1, NH_4^+ = 0.5, NO_3^- = 0.5, and PO_4^{3-} = 0.4 µmol L^{-1}), but NO_3^- and $Si(OH)_4$ increased with depth (Fig. 2e-f). There was a significant ($p < 0.01$), positive correlation ($r^2 = 0.33$, $n = 26$) between the difference in potential density between 10 and 60 m depths versus the difference in nitrate concentrations at the same depths (Fig. 3). The potential density difference between two depths was used as a proxy for stratification. Other studies have applied a density difference between 5 and 80 m (Ardyna et al. 2013), but here it also relates to nutrient concentrations with 60 m closer to the nutricline, and 10 m was chosen to minimize surface effects.

3.2. PAR, chlorophyll a, NO_3, and salinity

At a representative CTD station (88° 53.78 N, 90° 53.25 E), the SML is clearly visible with an average salinity of 32.9 down to a depth of 27 m, from where salinity increased towards depths to a salinity of 33.7 at 60 m (Fig. 4). The salinity and thus density difference between the SML and the water below established a strong stratification of the water column with a potential density difference of 2.06 kg m^{-3} between 10 and 60 m depth. Temperature only increased by 0.04°C in this depth interval and did not enhance the stratification. Chl *a* was nearly uniform (0.24 mg m^{-3}) down to 27 m from where it gradually decreased to a constant background value of about 0.02 mg m^{-3} (Fig. 4). The Chl *a* profile is similar to those obtained in the Beaufort Sea (Laney et al., 2013), but note the clear absence of any sub-surface Chl *a* maxima which are frequent in other parts of the Arctic Ocean (Ardyna et al., 2013). The average NO_3^- concentration was 0.26 µmol L^{-1} in the SML (2-20 m) from where it increased towards depth and reached 3.44 µmol L^{-1} at 60 m (Fig. 4). PAR distribution in the water column was derived from the average PAR attenuation coefficient of K_d(PAR) of 0.17 m^{-1} at sea ice stations in August-September 2012, and an average under ice PAR value of 10.0 µmol m^{-2} s^{-1} (Lund-Hansen et al., 2015).

3.3. Quantum yield and nutrients

The maximum quantum yield parameter F_v/F_m was comparatively high in the water below the ice (Fig. 5a), with $F_v/F_m > 0.6$ for 63 percent of the samples, where values around 0.65 reflect optimum conditions for phytoplankton growth and a high photosynthetic activity (Schreiber, 2010; McMinn and Hegseth, 2004). Maximum yields were low (< 0.3) at a few stations but with no specific spatial variation, though parameters were only measured at sea ice stations (Fig. 1; Lund-Hansen et al., 2015). The mean maximum relative electron transfer rate $rETR_{max}$ of 13.8 ± 8.8 was low compared to other under-ice studies (Manes and Gradinger, 2009), but the low average light saturation point (E_k) of 63.6 ± 34.7 µM m^{-2} s^{-1} demonstrates that the phytoplankton was strongly acclimated to low light conditions (Boumann et al., 2018). The average 480:665 absorbance Chl *a* ratio was 1.38 and < 1.5 for > 80 percent of the samples. This indicates that the phytoplankton was not in a state of nutrient limitation as would be the case with an absorbance ratio > 2 (Heath et al., 1990). This corroborates an average SML (2-20 m) nitrogen pool of 0.61 µmol L^{-1}, which shows that nitrogen is low but not depleted in the SML. In any case, nitrogen was apparently the limiting nutrient with average Redfield N:P ratio of 3.1 in the SML (2-20 m) relative to P with a ratio > 6.6 at 40-60 depth (Fig. 6a). This is further supported by a low N:Si ratio of 0.6 in the SML (2-20 m) (Fig. 6b) where a ratio of 4 would indicate that Si is the limiting nutrient (Gilpin et al., 2004).

3.4 Primary production in the Amundsen Basin in late July and autumn 2012

The significant differences in nutrient concentrations, especially in NO_3- and $Si(OH)_4$, between the SML and deeper waters indicates that nutrients have been depleted by the phytoplankton (Fig. 2e-f), and at a time prior to our sampling in August/September. This primary production was estimated based on differences in nutrient concentrations between the surface layer and the bottom of the winter mixed layer at 60 m following Codispoti et al. (2013). Using a C:N-ratio of 6.6, a vertical integration of the water column to the bottom of the photic zone (27 m; 1 percent PAR) resulted in a bloom primary production estimate of 67.5 mg C m^{-2} d^{-1}. It is unknown when this bloom in the water column took place but presumably in mid-late July and following sea ice-related blooms beginning July as observed in the Canadian Basin (Leu et al., 2011). In August-September we calculated the primary production in the water column to be 3.9 mg C m^{-2} d^{-1} derived from eq. A2 (disregarding nitrate limitation). This was based on a carbon flux of 1.8 mg C m^{-2} d^{-1}, model vertical nitrogen flux of 0.02 mmol NO_3^- m^{-2} d^{-1}, and a C:N ratio = 6.6 for August-September (Tab. 1).

3.5. Primary production in the Amundsen Basin in an sea ice-free setting

The model simulated the environmental conditions in the upper 50 m of surface waters for a future ice-free period in July and August. Meteorological conditions for 2012 showed that air temperatures during summer were close to 0°C until the end of August and wind speeds were relatively low during July-August with an average of 4.8 m s^{-1}, except for some peaks with velocities of up to 10 m s^{-1} (Fig. 7a). Surface PAR was estimated to decrease slightly over time from about 400 µmol m^{-2} s^{-1} in the beginning of July to 200 µmol m^{-2} s^{-1} in the end of August with a peak value of about 600 µmol m^{-2} s^{-1} expected for mid-July (Fig. 7b). These PAR values are in accordance with *in situ* measurements in August (Fernández-Méndez et al., 2015; Lund-Hansen et al., 2015). Model results showed an increase in sea surface temperatures from -1.6 to 1.6 °C during July and August (Fig. 7c). The strong halocline will remain intact all through the ice-free period with a deepening of the 30.80 isohaline related to wind induced shorter mixing events like in mid-July (Fig. 7e). Water column stratification increased by 0.11 kg m^{-3} during an ice-free July-August due to heating, expressed as a density differences between 10 and 35 m depths beginning July and mid-August. Model results showed an uptake of nitrate in the SML with relatively high (0.2 mg m^{-3}) Chl *a* concentrations in the beginning of July, and a stronger nitracline development over time (Fig. 7d). Chl *a* concentrations will decrease over time above the nitracline with concentrations about 0.08 mg m^{-3} in the end of August (Fig. 7d). There will be a clear downwards displacement of the nitracline in mid-July with raised Chl *a* in the surface layer caused by increased wind mixing during the 17 days period of increased wind speeds (8-9 m s^{-1}) in mid-July (Fig. 7a-d). Other periods of increased Chl *a* as in the end of July, and 23-24 August were likewise related to periods of raised wind speeds (Fig. 7a-d) and accordingly increased nitrate fluxes. Average nitrate fluxes at 10 m depth were 6 times higher during the ice-free July-August period of 0.12 mmol NO_3^- m^{-2} d^{-1} compared to a flux of 0.02 mmol NO_3^- m^{-2} d^{-1} below the sea ice cover (Tab. 1).

The modeled primary production was analyzed for two scenarios with ice-free conditions of different lengths and timing: an ice-free August and an ice-free July-August. Results showed a high initial primary production of about 150 mg C m^{-2} d^{-1} for both August and July-August scenarios when the water column was exposed to high light at a sudden. Afterwards, the production gradually decreased over time to a level of 50-60 mg C m^{-2} d^{-1} (Fig. 7e). However, for July-August there was a period of increased primary production in July, where production increased from about 50 to 120 mg C m^{-2} d^{-1} which was clearly related to the period of high wind speeds, high Chl *a*, and increased vertical mixing, as outlined above. The average primary production for the two first scenarios was 37.4 and 55.2 mg C m^{-2} d^{-1} for each of the two ice-free periods in August and July-August, respectively. Hence, this strongly indicates that the primary production will increase 10 to 14 times in the western Amundsen Basin when August or July-

August are sea ice free as compared to a present August primary production of 3.9 mg C m^{-2} d^{-1} below the sea ice. The increase in surface PAR by 100 percent in the model only increased primary production by 5 percent, which also points towards the importance of the vertical nutrient flux as the main limiting factor in the primary production.

4. Discussion

Primary production rates are low in the Amundsen Basin compared to other parts of the central Arctic Ocean. We demonstrated that the phytoplankton was in good physiological conditions for photosynthesis based on sufficient light and recycled nutrients, but also that flux of the production-limiting nitrate flux was inhibited by the strong stratification. Our model scenarios, asking whether primary production rates will increase in a future with no sea ice cover in summer in the Amundsen Basin, showed that rates will increase 10- to 14-fold.

4.1. Stratification in the Amundsen Basin

In late summer 2012, an approximately 20 m-thick surface mixed layer (SML) in the Amundsen Basin with reduced salinities, compared to more saline deeper waters, established a strong stratification of the water column. The average salinity difference reached 1.57 between 10 and 60 m depth, equal to a potential density difference of 1.30 kg m^{-3}. Similar water column density differences are often found near estuaries (Lund-Hansen et al., 1996) and other freshwater-influenced coastal locations (Simpson, 1995). Stratification is a balance between forces that enhance stratification, such as freshwater inflow and surface heating, and forces that reduce stratification, like wind and currents, by adding kinetic energy that is needed to mix the water column (Simpson, 1995). Since a stratified water column strongly inhibits vertical mixing and thereby also the flux of nutrients into the photic zone (Sharpless et al., 2007), any foreseen changes in the stratification of the Amundsen Basin will affect nitrate fluxes and effectively the primary production of the Arctic Ocean, as observed in the Canada Basin (Carmack et al., 2004). There is an ongoing increase in the freshwater runoff to the Arctic Ocean because of an increased precipitation in the catchment areas (Carmack et al., 2015; Peterson et al., 2002). Climate models predict that this increase in runoff will continue (Nummelin et al., 2016) whereby the freshwater component in the stratification balance will increase in the future. An increased freshwater inflow could also enhance the transport of nutrients from surrounding continents to the Arctic Ocean in favor of increased primary production. However, Carmack et al. (2015) showed that nutrients advected with the freshwater were consumed in the shelf areas before they reached the central Arctic Ocean. Hence, new nutrients for primary production will likely not be available in the central Arctic Ocean. Solar-induced heating of the water is regarded as a constant in the stratification balance. Forces that reduce stratification, like currents, are generally low in the central Arctic Ocean < 0.03-0.05 m s^{-1} (Bluhm et al., 2015) and are accordingly not expected to reduce stratification significantly. This leaves the wind to be the main parameter that might reduce the stratification. However, winds are generally low (average wind speed at 10 m altitude: 3.2 m s^{-1}; Jakobson et al., 2012) and comparable to the wind time-series from Kalnay et al. (1996) that was used in the present model. For a summer ice-free Amundsen Basin scenario, our model predicted events of higher winds and increased mixing in July and August and a potential increased flux and transport of nutrients into the surface water, though inhibited by the strong stratification. Comparable increased wind mixing during sea ice melting and in waters that are free of sea ice was observed in other studies (Yang et al., 2004). There are, however, no indications that wind speeds will increase in the Arctic in the future, as atmospheric re-analyses have demonstrated that summer (June-September) wind speeds in the Arctic Ocean actually decreased during 1992-2000, but remained unchanged in the central Arctic Ocean between 2000 and 2009 (Spreen et al., 2011). Hence, we do not expect a weakening of the water column stratification in summer in the future. A study of turbulent kinetic energy, mixing and ice-free

conditions in the central Canada Basin also concluded that stratification continued to suppress wind induced mixing when ice-free (Lincoln et al., 2016), thus supporting our results from the Amundsen Basin.

4.2. Present and future ice-free primary production in the Amundsen Basin

Results showed primary production rates in the Amundsen Basin of 67.5 mg C m^{-2} d^{-1} as based on the Codispoti et al. (2013) method of a nutrient concentration difference between the surface and winter mixed layer. It is assumed that this bloom occurred mid-July around the time of maximum surface PAR, and proceeded until most nutrients were depleted from the surface layer. Following this bloom the production decreased to 3.9 mg C m^{-2} d^{-1}, based on nutrients, Chl *a*, and PAR from a representative station during August-September 2012, and which compares to the primary production by sea ice algae of 4.2 mg C m^{-2} d^{-1} measured in the Amundsen Basin in August-September 2012 (Fernandez-Mendez et al., 2015). The 3.9 mg C m^{-2} d^{-1} rate is supposedly based on recycled ammonium in the SML with a very limited new and nitrate-based production. This assumption relies on the very low production rate, the occurrence of a very strong salinity mediated density interface, and accordingly a reduced vertical transport of nutrients from nutrient rich waters below the pycnocline.

Our model simulated ice-free conditions in the Amundsen Basin with on-site meteorological boundary conditions and starting conditions based on *in situ* observations. It estimated primary production rates of 37.4 mg C m^{-2} d^{-1} for an ice-free August and rates of 55.2 mg C m^{-2} d^{-1} for an ice-free July and August, which are 10 and 14 times higher than the present 3.9 mg C m^{-2} d^{-1}. The current increases in primary production in the Amundsen Basin are consistent with other pan-Arctic studies of primary production in an ice-free Arctic Ocean (Zhang et al., 2010; Hill, et al., 2013). The rates are, on the other hand, lower than current below-ice primary production rates of 106 mg C m^{-2} d^{-1} in the Canada Basin (Lee and Whitledge, 2005) and the whole Arctic Basin of 117 mg C m^{-2} d^{-1} (Rao and Platt, 1984). This points towards a generally low primary production in the Amundsen Basin both under the sea ice and in a future ice-free situation. Hence, why is this the case, and what are the limiting parameters for the primary production in Amundsen Basin? It is generally assumed that light is the main limiting factor for ice algae primary production (Leu et al., 2011) and pelagic Arctic primary production (Arrigo and Dijken, 2011) during spring and early summer. Later in the season, most of the nutrients in the surface waters have been assimilated and a pycnocline develops, whereby nutrient availability limits the primary production (Sakshaug, 2004). In spite of the lower below-ice PAR levels in August-September 2012 of about 10 µmol m^{-2} s^{-1} and a low (0.1) transmittance (Lund-Hansen et al., 2015), phytoplankton are well-adapted to this low light by having a high average maximum quantum yield of $F_v/F_m = 0.52 \pm 0.15$. This yield expresses the ability or potential of the phytoplankton to conduct photosynthesis and numbers of 0.65 in marine phytoplankton are considered to be high (Schreiber et al., 1995; McMinn and Hegseth, 2004). Also the low light saturation point of $E_k = 62.6 \pm 36.8$ µmol m^{-2} s^{-1} demonstrated the acclimation of phytoplankton to the low prevailing PAR. Such a light saturation point is typical for Arctic waters (Hout et al., 2013; Boumann et al., 2018) and a similar value ($E_k = 41$ µmol m^{-2} s^{-1}) was independently measured by Fernández-Méndez et al. (2015) in the Amundsen Basin in August-September 2012. The average 480:665 absorbance Chl *a* ratio of 1.38 indicated that the phytoplankton was not in a state of immediate nutrient limitation. It rather implies that despite the low nutrient concentrations there were still nutrients (likely recycled ammonia) in the water column available for photosynthesis (Heath et al., 1990). However, the ratio can be affected by differences in algae species composition (*op cit.*) but these are supposedly of minor importance compared to the significantly low ratio of 1.38. Further, phytoplankton diversity is comparatively low in the Arctic Basins, dominated by dinoflagellates and diatoms in July-August (Gosselin et al., 1997), and species composition is accordingly not likely to vary significantly between our stations. Nevertheless, phytoplankton was

low-light adapted and the potential for photosynthesis was high, but primary production was only 3.9 mg C m^{-2} d^{-1} but increased to 37.4 mg C m^{-2} d^{-1} and 55.2 mg C m^{-2} d^{-1} for an ice-free August scenario and an ice-free July-August scenario, respectively. In the model, PAR increased from 10 µmol m^{-2} s^{-1} below the ice to an average of about 400 µmol m^{-2} s^{-1} at the ice-free sea surface, whereby production increased 10 and 14 times, whereas primary production only increased by 5 percent in a model scenario where the surface PAR (400 µmol m^{-2} s^{-1}) increased by 100 percent. This strongly supports that primary production in the ice-free periods was not limited by light but nutrient availability. This was further substantiated by the estimated increase in ice-free primary production that was driven by several events of wind-induced mixing of the upper part of the water column, and the related upwards transport of nitrate to the photic zone. The vertical nitrate flux increased correspondingly from 0.02 mmol NO_3^- m^{-2} d^{-1} below the sea ice to 0.06-0.12 mmol NO^- m^{-2} d^{-1} in the two sea ice-free scenarios, which corresponds to a production rates of 37.4 mg C m^{-2} d^{-1} for an ice-free August and 55.2 mg C m^{-2} d^{-1} for an ice-free July-August period. Low N:P and N:Si-ratios of 2-3 and 0.56, respectively, in the SML (2-10 m) support that nitrate was the limiting nutrient compared to both silicate and phosphate (Stratmann et al., 2017). This, in summary, strongly indicates that nutrients and specifically nitrate was the main limiting nutrient for primary production in the Amundsen Basin.

Conclusions

Primary production was low in the Amundsen Basin and seemingly lower compared to other Arctic Ocean deep water basins, and significantly lower than in surrounding shelf areas. In August-September 2012, a prominent surface mixed layer (SML) of reduced salinity was observed in the Amundsen Basin, which maintained a strong and significant stratification of the water column with notably low surface and high deep-water nutrient concentrations. Stratification inhibited vertical mixing, which limited primary production. Primary production in 2012 was estimated to be 67.5 mg C m^{-2} d^{-1} during the mid-summer phytoplankton bloom, but decreased to 3.9 mg C m^{-2} d^{-1} later in August and likely based on recycled ammonium. Based on the modeling, it was concluded that primary production in the Amundsen Basin in future ice-free conditions will increase to about 37.4 and 55.2 mg C m^{-2} d^{-1} in August and July-August, respectively.

Appendix A

Model descriptions

The one-dimensional model is based on the COHERENS ocean model (Luyten et al., 2014). Due to the limited observations in the area, a new simple biogeochemical model based on a more complex ecosystem model applied for the subtropical Atlantic (Richardson and Bendtsen, 2017) is included in the model. Boundary conditions for momentum are determined by the wind stress and a no-flux condition at the bottom. Boundary conditions for temperature and salinity are determined by surface fluxes of energy and precipitation and a no-flux condition at the bottom of the water column. The transport equation for biogeochemical tracers (φ) is defined by:

$$\partial\varphi/\partial t = \partial k_v/\partial z \, \partial\varphi/\partial z + S(\varphi) \quad (A.1)$$

where a no-flux condition is applied both at the surface and at the bottom. The vertical turbulent diffusion coefficient (k_v) is determined by a k-ε turbulence scheme and it includes a constant diffusion coefficient of $5 \cdot 10^{-5}$ m^2 s^{-1}, assuming that it represents a low background mixing in the area. Internal sinks and sources (S(φ)) are defined below. Conditions in the upper 200 m (applying a vertical spacing of 2 m) was integrated with a time step of 20 minutes. Meteorological forcing with a time step of 6 hours.

It was assumed that there was no wind or atmospheric heat exchange on the sea surface during

ice-covered periods and the influence from melting and freezing of sea ice on salinity and temperature was also ignored. Initial conditions were based on observed under-ice distributions in August of temperature, salinity, nitrate, and Chl *a* was related to biomass (P) by applying a constant Chl *a*:carbon ratio of 1:48 (g g^{-1}) (Richardson and Bendtsen, 2017). Nitrate (DIN) was assumed to be the limiting nutrient for phytoplankton growth. Particulate and dissolved organic nitrogen fractions (PON and DON) were produced from phytoplankton mortality and grazing. Photosynthesis (Prod) is limited by light (PAR) and nutrients (DIN):

$$PP(z) = chl(z)P^{B}_{max}\left(1-\exp\left(\frac{-PAR(z)\alpha^{B}}{P^{B}_{max}}\right)\right)\frac{DIN}{k_{DIN}+DIN} \qquad \text{(A.2)}$$

where chl(z) is chlorophyll a, P^{B}_{max} and α^{B} are the photosynthetic parameters and k is a half saturation constant for nitrate (0.01 mmol N m^{-3}). P^{B}_{max} and α^{B} are obtained from an ice-free area in August 2012 (Fernández-Mendéz et al., 2015). Photosynthesis below the ice was calculated from under ice PAR and water column attenuation coefficient K_d(PAR) (Lund-Hansen et al., 2015).Primary production (PP) is obtained by vertically integrating Prod(z) in the euphotic zone. Sink and source terms for the ecosystem state variables are defined as:

$\partial P/\partial t = \eta_{N:C}$ Prod- mP – G (A.3)

$\partial DIN/\partial t = - \eta_{N:C}$ Prod + 1/τ (PON+DON) (A.4)

$\partial PON/\partial t = (1-\delta DOM)$ mP + (1- γDOM) G - 1/τ PON – ws $\partial PON/\partial z$….(A.5)

$\partial DON/\partial t = \delta DOM$ mP + γDOM G - 1/τ DON (A.6)

A Redfield ratio ($\eta_{N:C}$) of 16:106 is assumed between DIN and carbon and the phytoplankton mortality rate (m) is defined by a decay time scale of 20 days. Grazing (*G*) is calculated from a Holling-type III formulation (Adjou et al., 2012): $G = g_0 P^2/(g+P^2) Z$, ($g_0 = 1.6$ d^{-1}, $g = 0.05$ mmol N m^{-3}) where the zooplankton biomass is assumed to be related to the phytoplankton biomass as $Z = P^{\zeta}$ where $\zeta = 0.61$. A fraction ($\delta_{DOM} = 0.2$) of the mortality rate of phytoplankton adds to the DON pool and the remaining part is directed into PON. Similarly, a fraction ($\gamma_{DOM} = 0.2$) of the mortality from grazing contributes to DOM and the remaining part adds to the PON pool. The organic pools are assumed to remineralize to DIN with a constant time scale (τ) of 10 days, corresponding to typical remineralization time scales of oceanic labile organic matter in the surface layer (Bendtsen et al., 2015). Particulate organic carbon is assumed to sink through the water column with a constant sinking velocity (w_s) of 1 m d^{-1} (assumed to represent sinking of small phytoplankton cells). Model values are similar to values applied for the Atlantic (Richardson and Bendtsen, 2017) except for the photosynthetic parameters, where values from Arctic open water conditions in August 2012 (Fernández-Méndez et al., 2015) were applied, *i.e.* P^{B}_{max} = 3.5 (mg C (mg Chl *a*)$^{-1}$ h^{-1}) and $\alpha^{B} = 0.05$ (mg C (mg Chl *a*)$^{-1}$ h^{-1} (µmol m^{-2} s^{-1})$^{-1}$). The diffuse PAR attenuation coefficient of 0.17 m^{-1} was obtained from observations (Lund-Hansen et al., 2015).

The influence from tidal mixing below the ice was neglected as the dominating M_2-tidal influence from tidal mixing below the ice constituent was less than 0.05 m (Padman and Erofeeva, 2004), and the influence from ice-drift influence from tidal mixing below the ice on mixing in the surface layer was likewise assumed to be insignificant, compared to wind mixing influence from tidal mixing below the ice during the ice-free period.

Acknowledgements

Brdr. Hartmann's Foundation and the Carlsberg Foundation are thanked for the financial support. influence from tidal mixing below the ice SMO was supported by the Blue-Action project, which has received funding from the EU Horizon influence from tidal mixing below the ice

2020 research and innovation program - grant agreement No. 727852. The helicopter team, influence from tidal mixing below the ice Captain, and crew of icebreaker *Oden*, the Continental Shelf Project, and especially cruise leader influence from tidal mixing below the ice Christian Marcussen, GEUS, Denmark are all thanked for the successful LOMROG III cruise and influence from tidal mixing below the ice very good cooperation.

Table 1. Estimated primary production (mg C m^{-2} d^{-1}) during bloom based on observations of influence from tidal mixing below the ice nitrate. Model solutions of vertical turbulent diffusive nitrate (F_N) and carbon fluxes (F_c, calculated influence from tidal mixing below the ice from F_N and a C:N ratio of 6.6) and primary production in three scenarios: (1) sea ice covered, (2) influence from tidal mixing below the ice ice-free in August and (3) ice-free in July-August. Nitrate fluxes and primary production are influence from tidal mixing below the ice averaged in the open-water period.

	N flux (mmol N m^{-2} d^{-1})	F_c (mg C m^{-2} d^{-1})	Production (mg C m^{-2} d^{-1})
Bloom	-	-	67.5
1: With sea ice	0.02	1.8	3.9
2: 1-30 August ice free	0.06	4.7	37.4
3: 1 July – 30 August ice free	0.12	8.7	55.2

Figure captions

Fig. 1. A) Arctic Ocean with sea ice extent at 17 September 2012, where the orange line is the median sea ice extent for September 1979-2000. Courtesy: National Snow and Ice Data Center, Boulder, Colorado, USA http://nsidc.org/arcticseaicenews/2012/09/ (right) CTD (red dots) and sea ice stations (black dots) in the Amundsen Basin in August-September 2012. Stations A (88° 03.58 N, 145° 16.56 E) and B (87° 28.24 N, 18° 58.52)

Fig. 2. a) Salinity, b) potential temperature θ (°C), c) fluorescence-based chlorophyll *a* concentration (mg m^{-3}), d) water sample chlorophyll *a* concentration (mg m^{-3}), e) nitrogen component NO_2^-, NH_4^+, NO_3^- concentrations (µmol L^{-1}), and f) PO^{3-} and $Si(OH)_4$ concentrations (µmol L^{-1}).

Fig. 3. Difference in potential density (kg m^{-3}) between 60 and 20 m depth versus difference in nitrate concentration (µmol L^{-1}), for the same depths at all CTD stations.

Fig. 4. Salinity, NO_3^- (µmol L^{-1}), chlorophyll *a* (mg m^{-3}), and Photosynthetic Active Radiation (PAR) at a representative CTD station (88° 53.78 N, 90° 53.25 E).

Fig. 5. a) Maximum quantum yield (F_v/F_m) measured below the ice against sampling dates (in Julian days), b) the 480:665 absorption ratio of phytoplankton samples against sampling dates (in Julian days).

Fig. 6. a) Average N:P - $(NO_2^- + NH_4^+ + NO^-):(PO_4^{3-})$ and b) N:Si - $(NO^- + NH_4^+ + NO_3^-):(Si(OH_4)$ ratios with depth.

Fig. 7. a) Meteorological model forcing and derived fields, based on re-analysis data. a) Wind speed ($m\ s^{-1}$) and air temperature (°C), b) surface Photosynthetic Active Radiation (PAR) ($\mu mol\ m^{-2}\ s^{-1}$). Model solutions in the July-August ice-free scenario of c) temperature (°C) (contour lines of salinity) and d) Chl *a* ($mg\ m^{-3}$) (contour lines of NO_3 ($\mu mol\ L^{-1}$)), e) Primary production ($mg\ C\ m^{-2}\ d^{-1}$) for the two scenarios: July-August (solid line), and August (dotted line).

References

Ardyna, M., Gosselin, M., Michel, C., Poulin, M., Tremblay, J.-É., 2011. Environmental forcing of phytoplankton community structure and function in the Canadian High Arctic: contrasting oligotrophic and eutrophic regions. Mar. Ecol. Prog. Ser. 442, 37-57, https://doi.org/10.3354/meps09378

Ardyna, M., Babin, M., Gosselin, M., Devred, E., Bélanger, S., Matsuoka, P., Tremblay, J.-É., 2013. Parameterization of vertical chlorophyll a in the Arctic Ocean: impact of the subsurface chlorophyll maximum on regional, seasonal, and annual primary production estimates. Biogeosciences, 10, 4383-4404, https://doi:10.5195/bg-10-4383-2013.

Ardyna, M., Babin, M., Gosselin, M., Devred, E., Rainville, L., Tremblay, J.-É., 2014. Recent Arctic Ocean sea-ice loss triggers novel fall phytoplankton blooms. Geophys. Res. Lett. 41, 6207-6212, https://doi.org/10.1002/2014GL061047

Adjou, M., Bendtsen, J., Richardson, K., 2012. Modeling the influence from ocean transport, mixing and grazing on phytoplankton diversity. Ecol. Modell. 225, 19-27, https://doi.org/10.1016/j.ecolmodel.2011.11.005.

Arrigo, K.R., Dijken, G. L., 2011. Secular trends in Arctic Ocean net primary production. J. Geophys. Res. 116, C09011, https://doi.org/10.1029/2011/JC007151

Arrigo, K.R., Dijken, G.L., 2015. Continued increases in Arctic Ocean primary production. Prog. Ocean. 136, 60-70, https://doi.org/10.1016/j.pocean.2015.05.002.

Barber, D.G., Hop, H., Mundy, C.J., Else, B., Dmitrenko, I.A., Tremblay, J.-E., Ehn, J.K., Assmy, P., Daase, M., Candlish, L.M., Rysgaard, S., 2015. Selected physical, biological and biogeochemical implications of a rapidly changing Arctic Marginal Ice Zone. Prog. Ocean. 139, 122-150. https://doi.org/10.1017/j.pocean.2015.09.03

Bendtsen, J., Hilligsøe, K. M., Hansen, J. L. S., Richardson, K., 2015. Analysis of remineralisation, lability, temperature sensitivity and structural composition of organic matter from the upper ocean. Prog. Ocean. 130, 125-145, https://doi.org/10.1016/j.pocean.2014.10.009

Bluhm, B.A., Kosobokova, K.N., Carmack, E.C., 2015. A tale of two basins: An integrated physical and biological perspective of the deep Arctic Ocean. Prog. Ocean. 139, 89-121, https://doi.org/10.1016/j.pocean.2015.07.011

Bouman, H.A., Platt, T., Doblin, M., Figueiras, F.G., Gudmundson, K., Gudfinsson, H.G., Huang, B., Hickman, A., Hiscock, M., Jackson, T., Lutz, V.A., Mélin, F., Rey, F., Pepin, P., Segura, V., Tilstone, G.H., Dongen-Vogels, V., Sathyendranath, S., 2018. Photosynthesis-irradiance parameters of marine phytoplankton: synthesis of a global data set. Earth. Syst. Sci. Data. 10, 251-266, https://doi.org/10.5194/essd-10-251-2018

Carmack, E.C., Macdonald, R.W., Jasper, S. 2004. Phytoplankton productivity on the Canadian shelf of the Beaufort Sea. Mar. Ecol. Progr. Ser. 277, 37-50. https://doi.org/ 10.3354/meps277037.

Carmack, E.C., Yamamoto-Kawai, M., Haine, T.W.N., Bacon, S., Bluhm, B.A., Lique, C., Melling, H., Polyakov, Straneo, L.V., Timmermanns, M.-L., Williams, W.J., 2015. Freshwater and its role in the Arctic marine system: Sources, disposition, storage, export, and physical and biogeochemical consequences in the Arctic and global oceans, J. Geophys. Res. Biogeosci. 121, 675-717, https://doi.org/10.1002/2015JG003140.

Codispoti, L.A., Kelly, V., Thessen, A., Matrai, P., Suttles, S., Hill, V., Steele, M., Light, B., 2013. Synthesis of primary production in the Arctic Ocean: III. Nitrate and phosphate based estimates of net

community production. Prog. Ocean. 110, 126-150, https://doi.org/10.1016/j.pocean.2012.11.006.

Fernández-Méndez, M., Katlein, C., Rabe, B., Nicolaus, M., Peeken, I., Bakker, K., Flores, H. Boetius, A., 2015. Photosynthetic production in the central Arctic Ocean during the record sea ice minimum 2012. Biogeosci. 12, 3525-3549, https://doi.org/10.5194/bg-12-3525-2015.

Gilpin, L.C., Davidson, K., Roberts, E., 2004. The influence of changes in nitrogen:silicon ratios on diatom growth dynamics. J. Sea Res. 51, 21-35, https://doi.org/10.1016/j.seares.2003.05.005.

Gosselin, M., Levasseur, M., Wheeler, P.A., Horner, R.A., Booth, B.C., 1997. New measurements of phytoplankton and ice algal production in the Arctic Ocean. Deep-Sea Res. II, 44, 1623-1644, https://doi.org/10.1016/S0967-0645(97)00054-4.

Hansen, H.P., Koroleff, E., 1999. Determination of nutrients. In: Grasshoff, K., Ehrhardt, M. (Eds.), Methods of seawater analysis. 3rd Edition. Wiley-VCH, Germany, pp. 159-228. Hawes, I., Lund-Hansen, L.C., Sorrell, B.K., Nielsen, M.H., Borzák, R., Buss, I., 2012. Photobiology of sea ice algae during initial spring growth in Kangerlussuaq, West Greenland: insights from imaging variable chlorophyll fluorescence of ice cores. Photosyn. Res. 112, 103-115, https://doi.org/101007./s11120-012-9736-7.

Heath, M., Richardson, K., Kiørboe, T., 1990. Optical assessment of phytoplankton nutrient depletion. J. Plankton Res. 12, 381-396, https://doi.org/10.1093/plankt/12.2.245

Hill, V.J., Matrai, P.A., Olson, E., Suttles, S., Steele, S., Codispoti, L.A., Zimmermann, R.C., 2013. Synthesis of integrated primary production in the Arctic Ocean: II. In situ and remotely senses estimates. Prog. Ocean. 110, 107-125, https://doi.org/10.1016/j.pocean.2012.11.005

Huot, Y., Babin, M., Bruyant, F., 2013. Photosynthetic parameters in the Beaufort Sea in relation to the phytoplankton community structure. Biogeosciences, 10, 3445-3454, https://doi.org/10.5194/bg-10-3445-2013

Jakobson, E., Vihma, T., Palo, T., Jakobson, L., Keernik, H., Jaagus, J., 2012. Validation of atmospheric reanalysis over the central Arctic Ocean. Geophys. Res. Lett. L10802, https://doi.org/10.1029/20012GL051591

Jassby, A.D. Platt, T., 1976. Mathematical formulation of the relationship between photosynthesis and light for phytoplankton. Limnol. Ocean. 21, 540-547, https://doi.org/10.4319/lo.1976.21.4.0540

Jin, M., Popova, E.E., Zhang, J., Ji, R., Pendelton, D., Varpe, Ø., Yool, A., Lee, Y.J., 2015. Ecosystem model intercomparison of under-ice and total primary production in the Arctic Ocean. J. Geophys. Res, 121, 934-948, https://doi.org/10.1002/2015JCO11183.

Kalnay, E., Kanamitsu, M., Kistler, R., Collins, W., Deaven, D., Gandin, L., Iredell, M., Saha, S., White, G., Woollen, J., Zhu, Y., Chelliah, M., Ebisuzaka, W., Higgins, W., Janowiak, J., Mo, K.C., Ropelewski, C., Wang, J., Leetmaa, A., Reynolds, R., Jenne, R., Joseph, D., 1996. The NCEP/NCAR 40-Year Reanalysis Project. Bull. Amc. Met. Soc., 77, 437-471, https://doi.org/10.1175/1520-0477

Laliberté, F., Howell, S.E.L., Kushner, P.J., 2016. Regional variability of the projected sea ice-free Arctic during the summer months. Geophys. Res. Lett. 43, 256-263, https://doi.org/10.1002/2015GL066855.

Laney ,S.R., Krishfield, R.A., Toole, J.M., Hammar, T.R., Ashjian, C.J., Timmermans, M.-L., 2014. Assessing algal biomass and bio-optical distributions in perennially ice-covered polar ocean ecosystems. Polar Science, 8, 73-85, https://doi.org/10.1016/j.polar.2013.12.003

Laxon, S.W., Giles, K.A., Ridout, A.L., Wingham, D.J., Willatt, R., Cullen, R., Kwok, R., Schweiger, A., Zhang, Jinlun, Hass, C., Hendricks, S., Krishfield, R., Kurtz, N., Farrell, S., Davidson, M., 2013. Cryosat-estimates of Arctic Sea ice thickness and volume. Geophys Res. Lett., 40, 732-737, https://doi.org/10.1002/grl.50193.

Lee, S.H., Whitledge, T.E., 2005. Primary and new production in the deep Canada Basin during summer 2002. Pol. Biol. 28, 190-197. https://doi.org/0.1007/s00300-004-0676-3

Lee, S.H., Whitledge, T.E., Kang, S.H., 2007. Recent carbon and nitrogen uptake rates of phytoplankton in Bering Strait and the Chukchi Sea. Cont. Shelf Res. 27, 2231-2249. https://doi.org/10.1016/j.csr.2007.05.009

Leu, E., J.E. Søreide, D.O. Hessen, S. Falk-Petersen, Berge, J., 2011. Consequences of changing sea ice cover for primary and secondary producers in the European Arctic shelf seas: Timing, quantity, and quality. Progr. Oceanogr. 90, 18-32, https://doi.or/10.1016/j.pocean.2011.02.004.

Lincoln, B.J., Rippeth, T., Lenn, Y.-D., Timmermanns, M. L., Williams, W.J., Bacon, S., 2016. Wind- driven mixing at intermediate depths in an ice-free Arctic Ocean. Geophys. Res. Lett., 43, 9749- 9756, https://doi.org/10.1002/2016GLO70454.

Lund-Hansen, L.C., Skyum, P., Christiansen, C., 1996. Modes of stratification in a semi-enclosed bay at the North Sea-Baltic Sea transition. Est. Coast. Shelf Sci. 42, 45-54, https://doi.org/10.1006/ecss.1996.0004.

Lund-Hansen, L.C., Markager, S., Hancke, K., Stratmann, T., Rysgaard, S., Ramløv, H., Sorrell, B.K., 2015. Effects of sea ice light attenuation and CDOM absorption in the water below the Eurasian sector of central Arctic Ocean (> 88°N). Pol. Res. 34, 1-12, https://doi.org/10.3402/polar.v34.23978

Luyten, P., 2014. COHERENS – A coupled Hydrodynamical-Ecologicak Model for Regional and Shelf Seas: User Documentation. Version 2.6. RNINS Report, Operational Directorate Natural Environmen, Royal Belgian Institute of Natural Sciences. ftp://ftp.mumm.ac.be/patrick/coherens/training/Coherens_Training.pdf

Manes, S.S., Gradinger, R., 2009. Small scale vertical gradients of Arctic ice algal photo physiological properties. Photosyn. Res. 102, 53-66, https://doi.org/10.1007/s11120-009-9489-0.

McMinn, A., Hegseth, E.N., 2004. Quantum yield and photosynthetic parameters of marine microalgae from southern Arctic Ocean, Svalbard. J. Mar. Biol. Associ. UK 84, 865-871, https://doi.org/10.1017/S0025315404010112h.

Nummelin, A., Ilicak, M., Li, C., Smedsrud, L.H., 2016. Consequences of future increased Arctic runoff on arctic Ocean stratification, circulation, and sea ice cover. J. Geophys. Res. 121, https://doi.org/10.1002/2015JCO11156.

Olli, K., Wassmann, P., Reigstad, M., Ratkova, T.N., Arashkevich, E., Pasternak, A., Matrai, P.A., Knulst, J., Tranvik, L., Klais, R., & Jacobsen, A., 2007. The fate of production in the central Arctic Ocean – top-down regulation by zooplankton expatriates? Progr. Ocean. 72, 84-113, https://doi.org/10.1016/j.pocean.2006.08.002.

Overland, J.E., Wang, M., Walsh, J.E., Stroeve, J.C., 2013. Future Arctic climate change: Adaptations and mitigating time-scales. Earth's Future 2, 68- 74, https://doi.org/10.1002/2013EF000162

Padman, L., Erofeeva, S., 2004. A barotropic inverse tidal model for the Arctic Ocean. Geophys. Res. Let. 31, https://doi.org/10.1029/2003GL019003.

Peterson, B.J., Holes, R.M, McClelland, J.W., Vörösmarty, C.J., Lammers, R.B., Shiklomanov, A.I., Shiklomanov, I.A., Rahmstorf, S., 2002. Increasing river discharges to the Arctic Ocean. Science 298, https://doi.org/10.1126/science.1077445

Popova, E., Yool, A., Coward, A., Dupont, F., Deal, C., Elliot, S., Hunke, E., Jin, M., Steele, M., Zhang, J., 2012. What controls primary production in the Arctic Ocean? Results from an intercomparison of five general circulation models with biogeochemistry, J. Geophys. Res. 117, C00D12, https://doi.org/10.1029/2011JC07112.

Ralph, P.J., Gademann, R., 2005. Rapid light curves: A powerful tool to assess photosynthetic activity. Aqua. Bot. 82, 222-237, https://doi.org/10.1016/j.aquabot.2005.02.006.

Randelhoff, A., Fer, I., Sundfjord, A. ,Tremblay, J.-E., Reigstad, M., 2016. Vertical fluxes of nitrate in the

seasonal nitracline of the Atlantic Sector of the Arctic Ocean. J. Geophys Res. 121, 5282- 5295, https://doi.org/10.1002/2016JCO11779

Rao, D.V.S., Platt, T., 1984. Primary production of arctic waters. Pol. Biol. 3, 191-202, https://doi.org/10.1007/BF00292623

Rey, F., Skjoldal, H.R., Slagstad, D., 1987. Primary production in relation to climatic changes in the Barents Sea. In: Loeng, H. (Ed.), The effect of oceanographic conditions on the distribution and population dynamics of commercial fish stocks in the Barents Sea. Proceedings of the Third Soviet-Norwegian Symposium, Murmansk, 26-28 May 1986, pp. 29-46.

Richardson, K., Bendtsen, J., 2017. Photosynthetic oxygen production in a warmer ocean: The Sargasso Sea as a case study. Philos. Trans. Royal Soc. A 375:20160329, https://doi.org/10.1098/rsta.2016.0329.

Rudels, B., Anderson, L.G., Jones, E.P., 1996. Formation and evolution of the surface mixed layer and halocline of the Arctic Ocean, J. Geophys. Res. 101, 8807-8821, https://doi.org/10.1029/96JC00143.

Sakshaug, E., 2004. Primary and secondary production in the Arctic sea. In: The Organic Carbon Cycle in the Arctic Ocean (eds.) R. Stein and R.W. MacDonald. Springer, Berlin, 57-82, https://doi.org/10.1007/978-3-642-18912-8.

Schreiber, U., Hormann, H., Neubauer, C., Klughammer, C., 1995. Assessment of photosystem II photochemical quantum yield by chlorophyll fluorescence quenching analysis. Aust. J. Plant Phys. 22, 209-220, https://doi.org/10.1071/PP9950209.

Schreiber, U., 2010. Pulse-Amplitude-Modulation (PAM) Fluorometry and Saturation Pulse Method: an overview. In: Papageorgiou, C.G. and Govindjee (eds.): Chlorophyll a Fluorescence: A signature of Photosynthesis, pp- 279-319. Springer, Berlin.

Serreze, M. C., Holland, M.M., Stroeve, J., 2007. Perspectives on the Arctic's shrinking sea ice cover. Science 315, 1533-1536, https://doi.org/10.1126/science.1139426.

Serreze, M.C., Barry R., 2014. The Arctic Climate System. Cambridge University Press. pp 403. Serreze, M.C., Stroeve, J., Barrett, A.P., Boisvert, L.N., 2016. Summer atmospheric circulation anomalies over the Arctic Ocean and their influences on September sea ice extent: A cautionary tale. J. Geophys. Res. 121, https://doi.org/10.1002/2016JD025161.

Sharpless, J., Tweddle, J.F., Green, J.A.M., Palmer, M.R., Kim, Y.-N., Hickman, A.E., Holligan, P.M., Moore, C.M., Rippeth, T.P., Simpson, J.H., Krivtsov, V., 2007. Spring-neap modulation of internal tide-mixing and vertical nitrate fluxes at a shelf edge in summer. Limnol. Oceano. 52, 1735-1747, https://doi.org/10.4319/lo2007.52.5.1735

Slagstad, D., Ellingsen, I.H., Wassmann, P., 2011. Evaluating primary and secondary production in an Arctic Ocean void of summer sea ice: An experimental simulation approach. Progr. Ocean. 90, 117-131, https://doi.org/10.1016/j.pocean.2011.02.009.

Slagstad, D., Wassmann, P.F.J., Ellingsen, I., 2015. Physical constraints and productivity in the future Arctic Ocean. Front. Mar. Sci. 2, https://doi.org/10.3389/fmars.2015.00085.

Spreen, G., Kwok, R., Menemenlis, D., 2011. Trends in arctic sea ice drift and role f wind forcing: 1992-2009. Geophys. Res. Lett. 38, https://doi.org/10.1029/2011GL048970

Steinacher, M., Joos, F., Frölicjer, T.L., Bopp, L., Cadule, P., Cocco, V., Doney, S.C., Gehlen, M., Lindsay, K., Moore, J.K., Schneider, B., Segschneider, J., 2010. Projected 21st century decrease in marine productivity: A multi-model analysis. Biogeosciences 7, 979-1005, https://doi.org/10.5194/bg-7-979-2010.

Tremblay, J.-E. Gagnon, J., 2009. The effects of irradiance and nutrients supply on the productivity of Arctic waters: a perspective on climate change, 73-92, In: Nihoul, J.C.J. and A.G. Kostianoy (eds.). Influence of climate change on the changing sub-arctic conditions. The NATO Science for Peace and Security Programme. Springer, Berlin.

Tremblay, J.-E., Robert, D., Varela, D.E., Lovejoy, C., Darnis, G., Nelson, R.J., Sastri, A.R., 2012. Current state and trends in Canadian Arctic marine ecosystems: I. Primary production. Clim. Chan. 34, https://doi.org /10.1007/s10584-012-0496-3

Wheeler, P.A., Gosselin, M., Sheer, E., Thibault, D., Kirchman, D.L., Benner, R., & Whitledge, T.E, 1996. Active cycling of organic carbon in the central Arctic Ocean. Nature, 380, 697-699, https://doi.org.10.1038/380697

Yang, J., Comiso, J., Walsh, D., Krishfield, R., & Honjo, S., 2004. Storm-driven mixing and potential impact on the Arctic Ocean. J. Geophys. Res. 1009, https://doi.org/10.1029/200IJC001248

Zhang, J., Spitz, Y.H., Steele, M., Ashjian, C., Campbell, R., Berline, L., Matrai, P., 2010. Modeling the impact of declining sea ice on the Arctic marine planktonic ecosystem. J. Geophys. Res. 115, C10015, https://doi.org/10.1029/2009JC005387

Highlights:

1. Arctic Ocean – Amundsen Basin
2. Present and future ice-free primary production
3. Stratification inhibit primary production

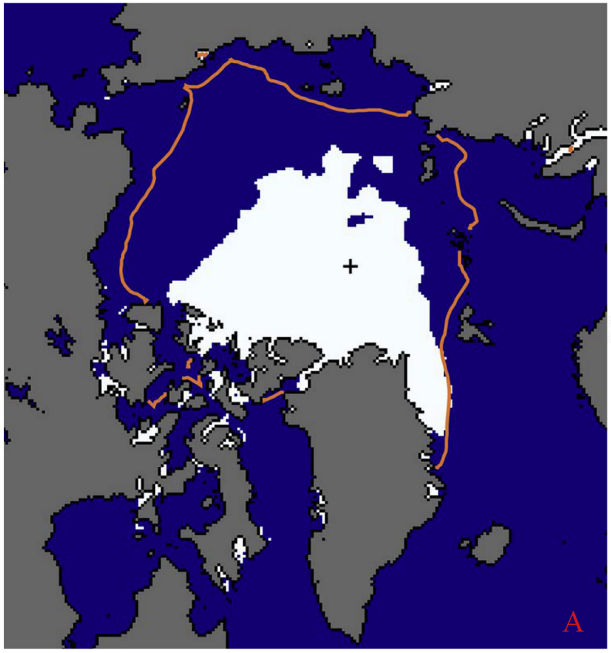
A

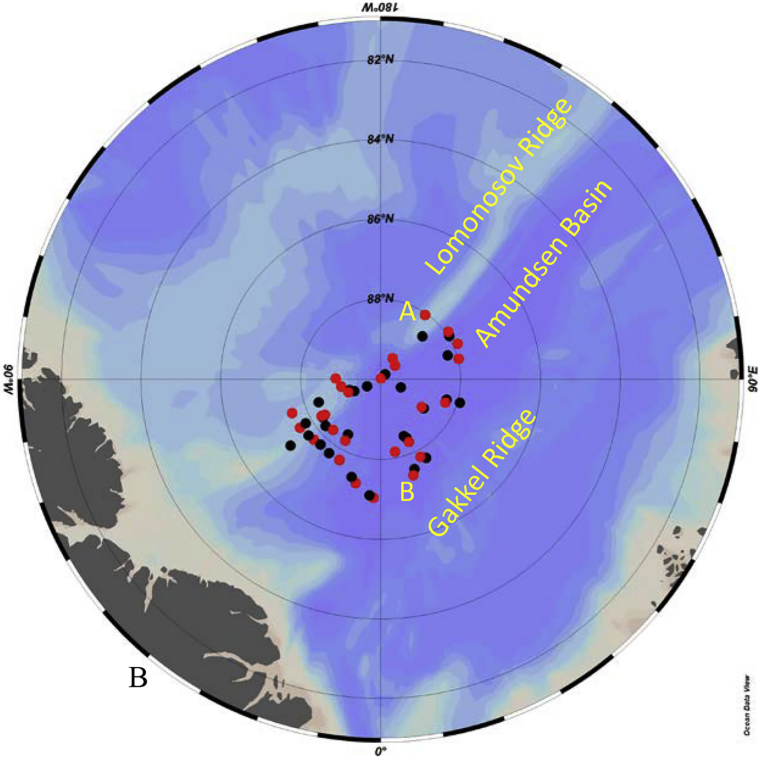
180°W
82°N
84°N
86°N
88°N
90°W
90°E
0°
Lomonosov Ridge
Amundsen Basin
Gakkel Ridge
A
B
Ocean Data View

B

Figure 1

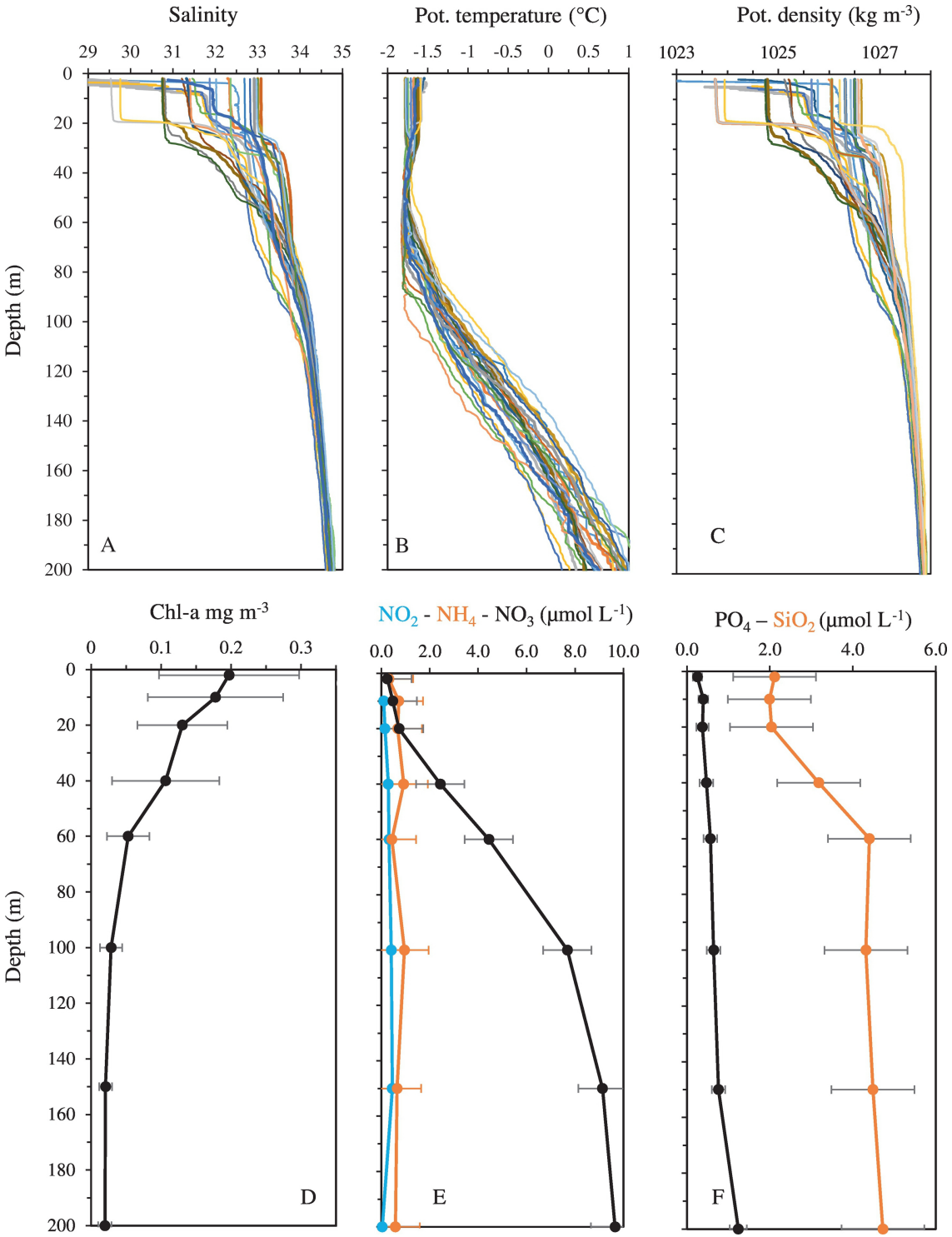
Salinity
29 30 31 32 33 34 35
Pot. temperature (°C)
-2 -1.5 -1 -0.5 0 0.5 1
Pot. density (kg m-3)
1023 1025 1027
Depth (m)
0 20 40 60 80 100 120 140 160 180 200
A
B
C
Chl-a mg m-3
0 0.1 0.2 0.3
NO2 - NH4 - NO3 (µmol L-1)
0.0 2.0 4.0 6.0 8.0 10.0
PO4 – SiO2 (µmol L-1)
0.0 2.0 4.0 6.0
Depth (m)
0 20 40 60 80 100 120 140 160 180 200
D
E
F

Figure 2

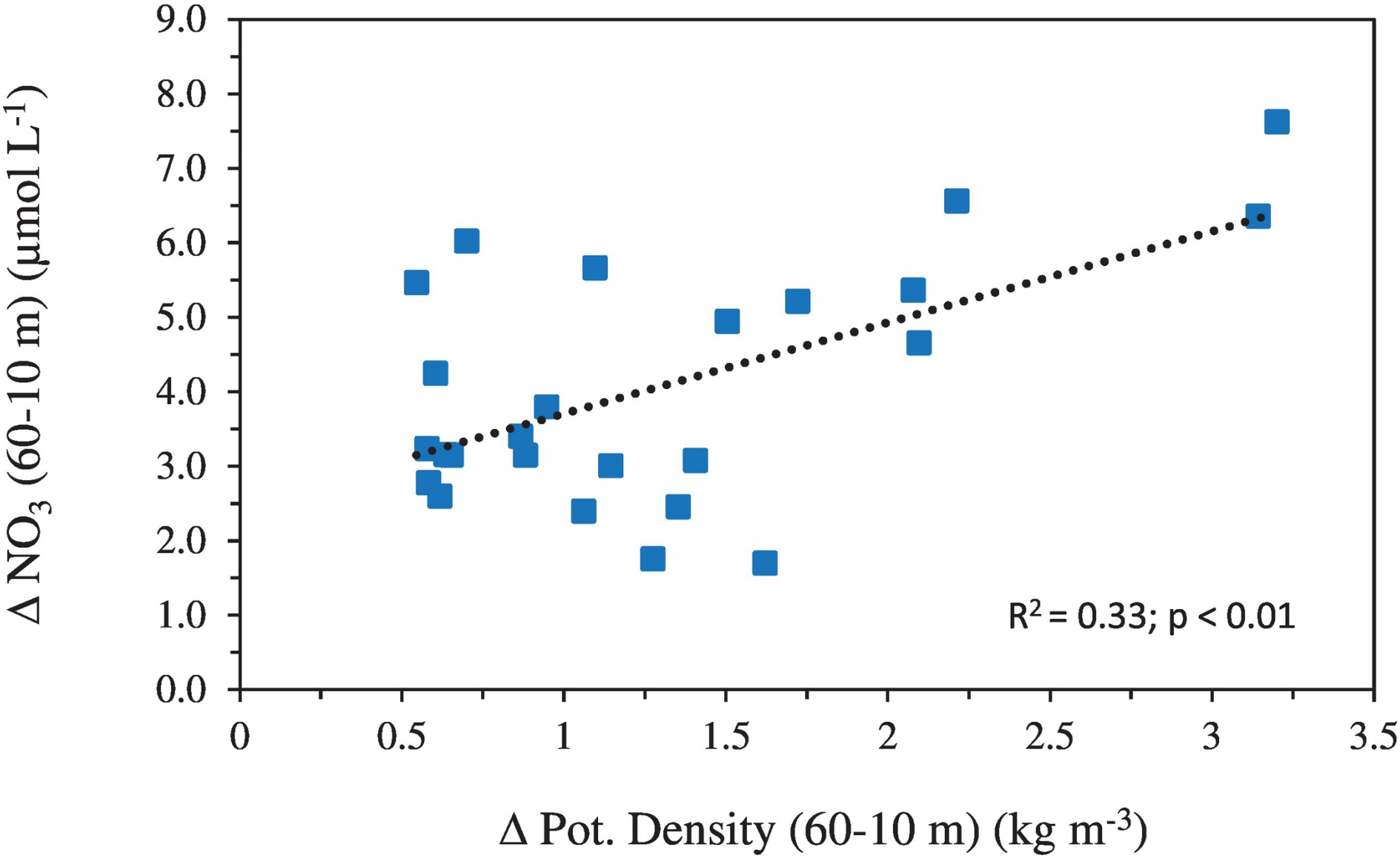
9.0
8.0
7.0
6.0
5.0
4.0
3.0
2.0
1.0
0.0
Δ NO3 (60-10 m) (µmol L-1)
0
0.5
1
1.5
2
2.5
3
3.5
Δ Pot. Density (60-10 m) (kg m-3)
R2 = 0.33; p < 0.01

Figure 3

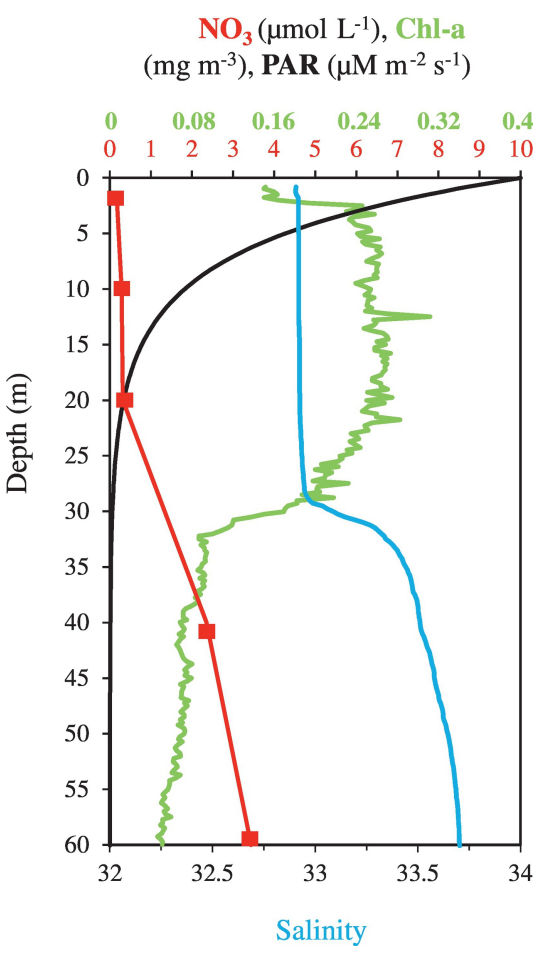
NO3 (µmol L-1), Chl-a
(mg m-3), PAR (µM m-2 s-1)
0
0.08
0.16
0.24
0.32
0.4
0 1 2 3 4 5 6 7 8 9 10
Depth (m)
0 5 10 15 20 25 30 35 40 45 50 55 60
32 32.5 33 33.5 34
Salinity

Figure 4

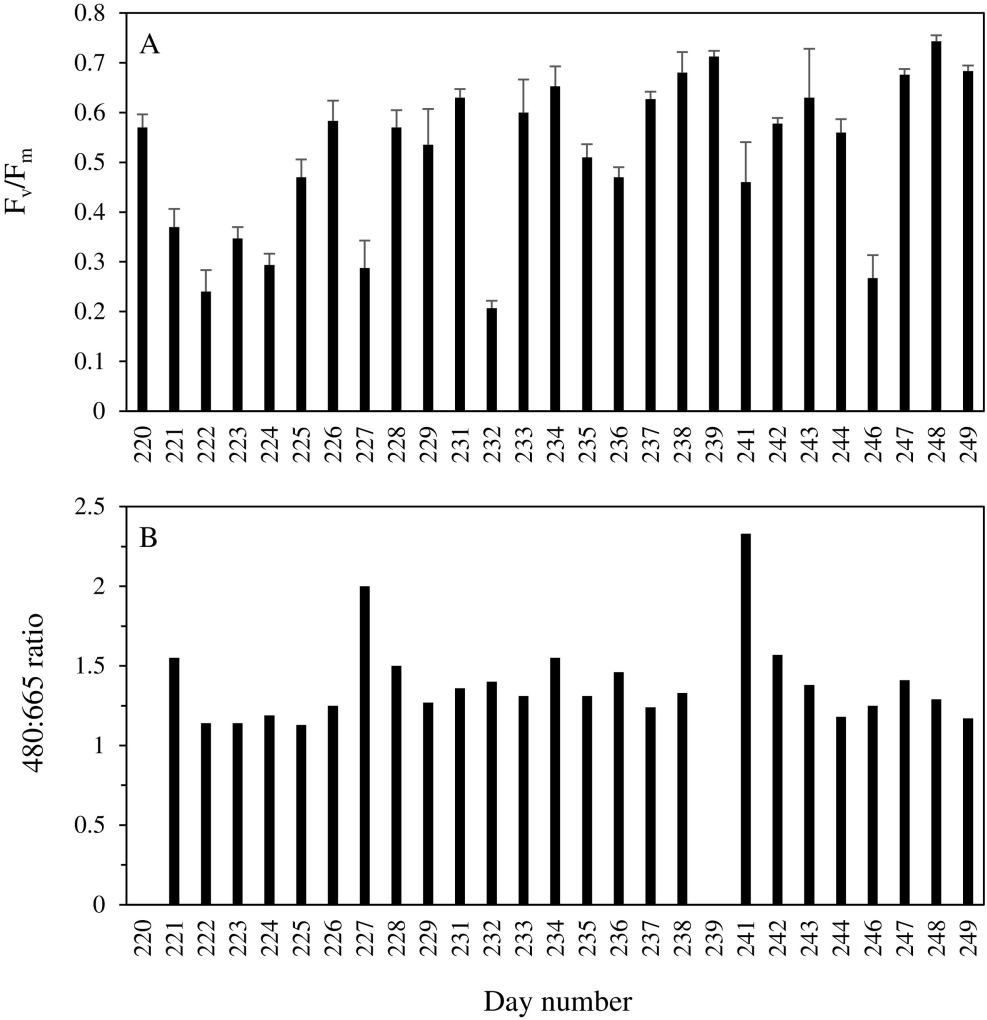
A
F_v/F_m
0.8
0.7
0.6
0.5
0.4
0.3
0.2
0.1
0
220 221 222 223 224 225 226 227 228 229 231 232 233 234 235 236 237 238 239 241 242 243 244 246 247 248 249
B
480:665 ratio
2.5
2
1.5
1
0.5
0
220 221 222 223 224 225 226 227 228 229 231 232 233 234 235 236 237 238 239 241 242 243 244 246 247 248 249
Day number

Figure 5

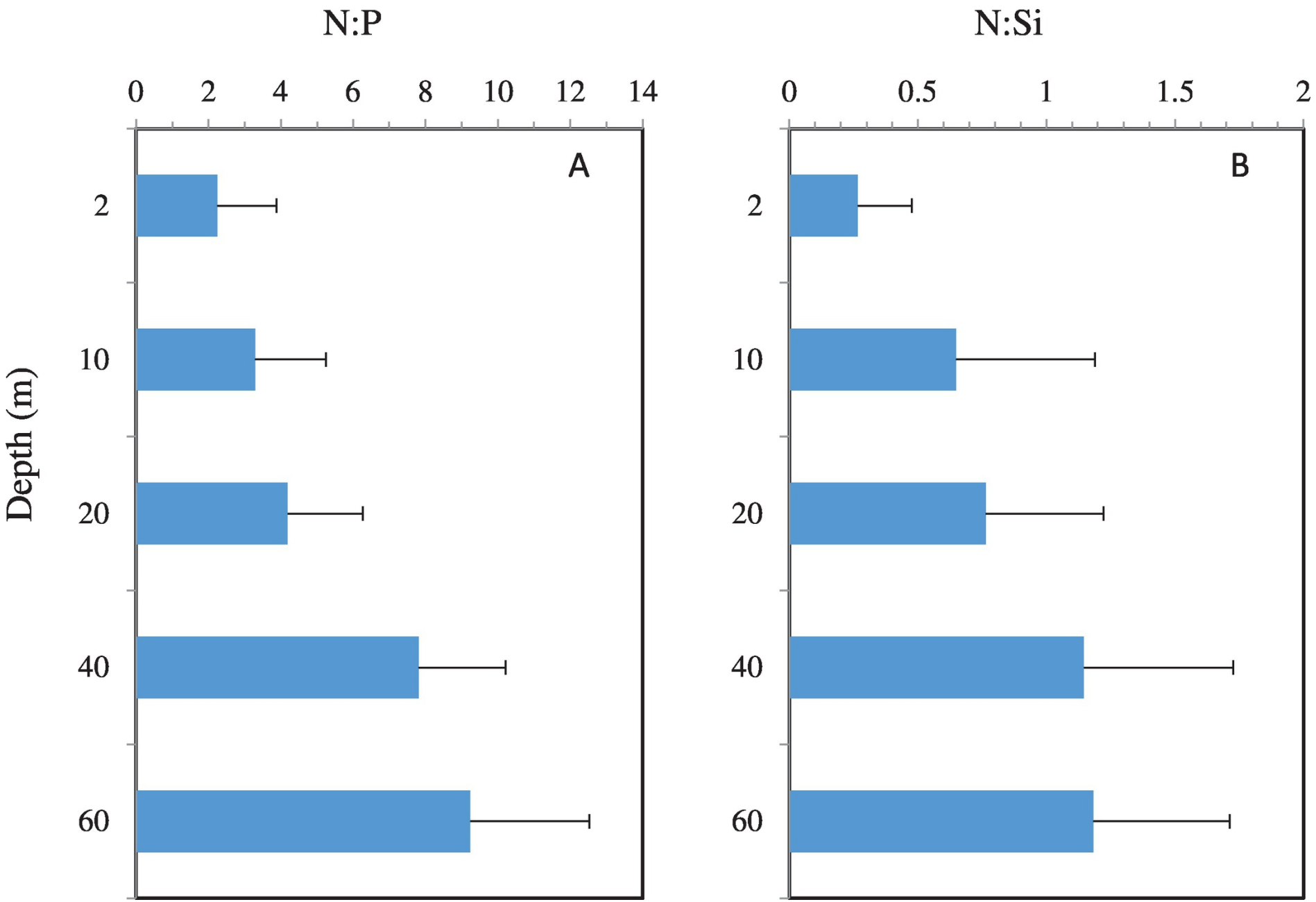

Figure 6

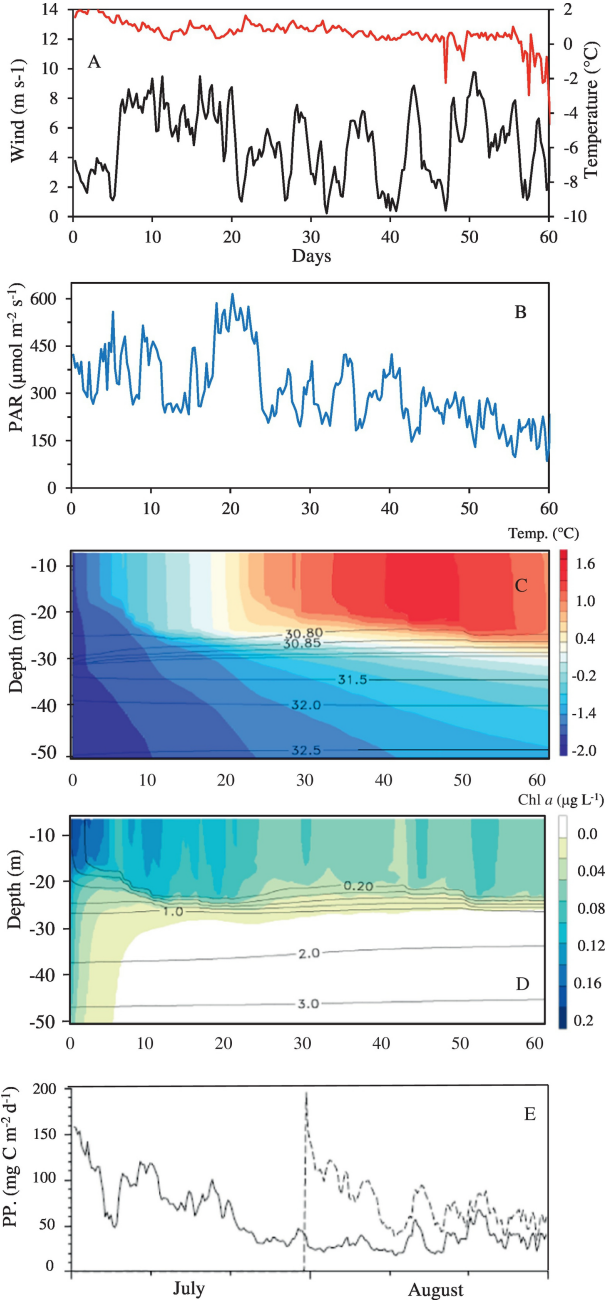
A
Wind (m s-1)
Temperature (°C)
Days
B
PAR (µmol m-2 s-1)
Temp. (°C)
C
Depth (m)
30.80
30.85
31.5
32.0
32.5
Chl a (µg L-1)
D
0.20
1.0
2.0
3.0
E
PP. (mg C m-2 d-1)
July
August

Figure 7